

Emplacement of the Anta Granite from Rio de Janeiro State (SE, Brazil); determined by magnetic fabrics

Odirney Benedito da Silva¹ , Maria Irene B. Raposo^{1*} 

Abstract

Magnetic fabric and rock magnetism studies were performed on the three facies of the Anta granite (SE of Rio de Janeiro State, southern Brazil). This intrusion is roughly elliptical (~ 14 km²), NE-SW oriented and composed of granodiorite, monzodiorite, quartz-diorite, syenogranite, and monzogranite. It shows solid-state deformation and tectonic foliation at its borders and is apparently isotropic in the central part where the internal fabrics are impossible or very difficult to measure through classical techniques. Magnetic fabrics were determined by applying both anisotropy of low-field magnetic susceptibility (AMS) and anisotropy of anhysteretic remanent magnetization (AARM). The AMS and AARM fabrics are coaxial for all facies. The parallelism between AMS and AARM tensors excludes the presence of a single domain (SD) effect in the AMS fabric. Several rock-magnetism experiments performed on one specimen from each facies show that, for all units, magnetic susceptibility and fabrics are carried by magnetite grains. Most of the magnetic foliations are steeply dipping in all facies, and are roughly parallel or sub-parallel to the foliation measured in the field and in the country rocks. In contrast, the magnetic lineations present mostly low plunges for almost the whole pluton, except for one site where it is steep (> 60°). Thin section analysis show that rocks from the borders of the Anta pluton are solid-state deformed, indicating that the borders of the pluton were affected by the regional strain during its emplacement. On the other hand, the lack of solid-state deformation at outcrop scale and in thin sections precludes deformation in the central part of the pluton to be determined, where igneous textures are preserved. This evidence allows us to interpret the magnetic fabrics observed in this part of the pluton as primary in origin (magmatic) and acquired when the rocks were solidified as a result of magma flow, in which steeply plunging magnetic lineation suggests that a feeder zone could underlain this area. Our data suggest that the regional deformation partially affected the emplacement of the Anta granite.

KEYWORDS: Magnetic Fabrics; anisotropy of low-field magnetic susceptibility; anisotropy of anhysteretic remanent magnetization; granite; Anta; Rio de Janeiro.

INTRODUCTION

The highlands of the Rio de Janeiro State are composed of granitic gneiss, paragneiss, and granite that are part of the Ribeira Belt. The Ribeira Belt, or Ribeira Orogen, is a Brasiliano/Pan-African orogenic belt located at the Mantiqueira Province (Almeida *et al.* 1981), with NE-SW structural trend, mostly controlled by NE high-angle strike-slip shear zones. This event was responsible for the generation of the voluminous granitic magmatism at Central Ribeira belt. The geodynamic evolution of the Ribeira belt took place during the amalgamation of the Western Gondwana, and was controlled by diachronic amalgamation of magmatic arcs, terranes, and cratons (Brito Neves *et al.* 1999, Campos Neto 2000, Trouw *et al.* 2000, Heilbron *et al.* 2004, Basei *et al.* 2010, Bento dos Santos *et al.* 2015). This belt represents a collisional orogen that has developed in several episodes of the convergence of the Brasiliana-Pan-African orogeny during the Neoproterozoic-Cambrian, with last stages occurring in the Lower Ordovician. Several studies on the Ribeira Belt

suggest that its granitoids are part of a Tonian to Ordovician orogenic belt and were generated at distinct collisional stages of the Brasiliano/Pan-African orogenic cycle (Machado *et al.* 1996, Trouw *et al.* 2000, Heilbron and Machado 2003, Silva *et al.* 2003, 2005, Tupinambá *et al.* 2012, Heilbron *et al.* 2013). The Ribeira belt in Rio de Janeiro State was divided into four tectonic domains separated by ductile shear zones, whose direction is parallel to the regional structures with predominantly horizontal slip (Machado *et al.* 2016). From SE to NW, the domains are: Litorâneo, Serra dos Orgãos, Paraíba do Sul, and Juiz de Fora (Fig. 1A). Based on geochronological data (Rb-Sr and U-Pb), the granitic magmatism was divided into three main groups (Machado *et al.* 2000); pre-, syn-, and post-collisional with ages ranging from 590 to 570, 560 to 530, and 520 to 480 Ma, respectively (Fig. 1A). In all tectonic domains there are orogenic, pre-, syn-, and post-collisional granitoid plutons with calc-alkaline to alkaline affinities. They were emplaced and/or reworked during intense magmatic activity during the stages of the Brasiliano (Pan-African) orogeny.

The majority of syn-tectonic granite plutons in the Ribeira belt, as is the case of the Anta granite, have characteristic such as solid-state deformation and tectonic foliation at its borders, while the central part of the pluton have such weak internal fabrics that it is impossible or very difficult to measure them through classical techniques based on direct field observations,

¹Instituto de Geociências da Universidade de São Paulo – São Paulo (SP), Brazil. E-mails: obsilva@usp.br, irene@usp.br

*Corresponding author.



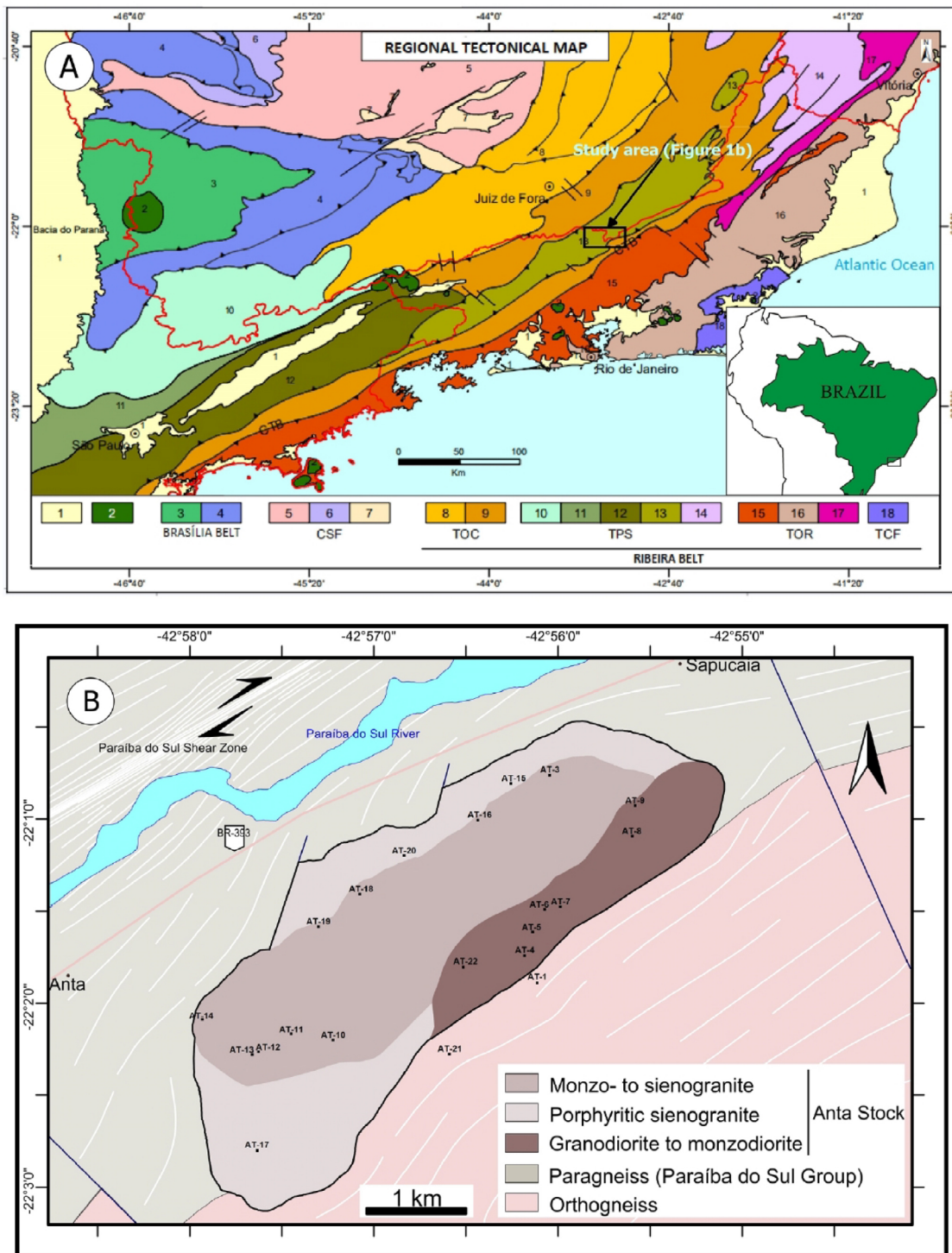


Figure 1. (A) Tectonic map of the central Ribeira belt showing the Anta granite. 1) Phanerozoic sedimentary basins; 2) Alkaline Plutons of the Upper Cretaceous and Paleogen; Brasília South Belt: 3) Nappe Guaxupé; 4) Nappe de Passos, Nappes Andrelândia System; Crátão São Francisco (CSF): 5) Archene and paleoproterozoic bases; 6) Neoproterozoic cover — Bambuí Group; 7) Mesoproterozoic to neoproterozoic meta-sedimentary sequences; Ribeira Strip: TOC-Western Terrain: 8) Lower Domain (Andrelândia); 9) Superior Domain (Judge from Outside); TPS-Paraíba do Sul Land: 10) Socorro Domain; 11) Domain Apiaí; 12) Embu Domain; 13) Paraíba do Sul Domain; 14) Cambuci Domain; TOR-Eastern Land: 15) Rio Negro Magmatic Arch; 16) Coastal Domain; 17) Domain Itálva; 18) TCF-Cabo Frio Land; CTB-Central Tectonic Limit (suture of the Ribeira Strip), after Heilbron *et al.* (2016). (B) Simplified geological map of the Anta Granite showing the sampled sites.

or in thin sections, and consequently these granites are often considered isotropic. On the other hand, it is important to understand the internal fabric of the granitic plutons, to investigate:

- their relationship with the regional structure;
- the magmatic flow;
- solid-state deformation.

In such cases, magnetic methods, especially the anisotropy of low-field magnetic susceptibility (AMS), have been widely used to determine the internal fabric of the plutons (e.g., Bouchez 1997). Magnetic anisotropy techniques are a powerful petro-physical tool that has been employed to determine planar (bedding, cleavage, and/or foliation) and linear (mineral lineations)

structural elements in sedimentary, metamorphic, and igneous rocks (for a review, see Tarling and Hrouda 1993, Borradaile and Henry 1997, Martín-Hernández *et al.* 2004, Herro-Bervera 2006, Martín-Hernández *et al.* 2009; and Almqvist *et al.* 2014). AMS is well suited for mapping magmatic foliations and lineations in igneous intrusions (e.g., Bouchez 1997, Archanjo *et al.* 1998, Archanjo *et al.* 2002, Trindade *et al.* 1999, Mamtani 2014, Sheibi and Majidi 2015, and references therein). The method can be applied even in rocks that are visually isotropic (Bouchez 1997). One of the distinct advantages of AMS measurements in granites is the ability to determine the lineation direction which is rarely observed in granites. The magnetic lineation is often inferred to indicate the stretching direction imposed by magma flow in igneous rocks (Tarling and Hrouda 1993, Borradaile and Henry 1997, Raposo *et al.* 2012; Bhatt *et al.* 2017, among many others). Numerous studies of AMS in granitoids have demonstrated a strong correlation between visible foliation and lineation and equivalent magnetic fabrics (Román-Berdiel *et al.* 1995, Archanjo *et al.* 1998, Esmaily *et al.* 2007, Raeisi *et al.* 2019, among many others).

Magnetic fabric can also be determined using anisotropy of anhysteretic remanent magnetization (AARM), which is not so popular in studies of granites as well in sedimentary rocks (Raposo *et al.* 2006, Oliva-Urcia *et al.* 2009, Raposo *et al.* 2014). This anisotropy isolates the contribution of remanence-bearing minerals from that of the paramagnetic and/or diamagnetic matrix. Since the ferromagnetic particles, which define the AARM tensor, and the paramagnetic and/or diamagnetic minerals may crystallize at different times with different orientations, the determination of the AARM allows an investigation of possibly overprinted fabrics.

To understand magmatic processes in plutons is one of the key problems because of the complexity of the geometric patterns and physical causes of magma flow. In many cases, the direct field evidence for large-scale flow has been erased from rock record (Trubač *et al.* 2009). The flow patterns may be inferred from the preserved mesoscopic fabrics acquired late in the magma chamber history along migrating crystallization fronts and easily reset by regional tectonic deformation (Benn *et al.* 1994, Paterson *et al.* 1998). The inference on the large-scale flow patterns within a pluton is difficult because of the poor strain memory of magmatic fabrics (Paterson *et al.* 1998). Late deformation makes new fabrics which may appear locally on large bodies, or can be more pervasive on smaller ones. These fabrics may modify or erase the earlier (primary) fabric depending on temperature and strain intensity. Indeed, granite pluton emplacement and deformation during the regional tectonic events is a hard study task, since granitic rocks do not always develop mesoscopic scale deformation fabrics. In syn-tectonic intrusions, the distinction between primary and secondary fabrics using microstructural observations may not be possible, considering that the emplacement of magmas is mostly controlled by the regional strain. In such a scenario, magmatic structures may have the same orientation of country rocks, even if a solid-state foliation is not strongly developed.

We have applied both AMS and AARM techniques to the Anta granite to determine the internal fabrics mainly of its

central part, since it is visually isotropic, to provide information on its emplacement, and to verify whether the whole body was affected by the regional strain. This granite has not been studied for any aspect, even geochemically, as show in this paper. In addition, it is the first granite from Rio de Janeiro State studied by magnetic methods. To better understand the magnetic fabrics we have also performed an extensive rock magnetism study.

GEOLOGICAL SETTING

The Anta granite is located in the border of the Paraíba do Sul shear zone, in the southwestern region of the state of Rio de Janeiro. This shear zone is one of the most important structures in the Central part of the Ribeira belt, which has been classically considered as a dextral shear zone developed in response to a transpressive regime which produced wide mylonitic zones (Corrêa Neto *et al.* 1993, Machado and Endo 1993). Stress directions determined from plagioclase fabrics has confirmed the kinematics of this deformation regime (Egydio-Silva and Mainprice 1999). After the magnetic fabrics determined in this paper, the Anta granite can now be associated to the group of granites of the Ribeira belt, which are smaller massifs, such as stocks or small tabular or elongated batholiths associated with regional high-angle ductile shear zones (Nummer 2001, Nummer *et al.* 2007). The plutons are foliated, with solid-state deformation at the borders and igneous flow structures in the central part. Contacts are often tectonically deformed and transposed to be concordant with host rock structures. I-type granites or granodiorites are predominant, although S-type granites are also found (Nummer *et al.* 2007).

The occurrence of a significant volume of granitic magmatism in the orogenic belt in Rio de Janeiro state can be explained by three geodynamic models (Nummer 2001):

- magmatic arc models associated with oceanic lithosphere subduction, which are described as the model formation of the Rio Negro Magmatic Suite in the Ribeira belt (Tupinambá 1999);
- island-arch/continent collision models, which are a case of extensive Brasiliana granitogenesis in the Proterozoic belt of the Mantiqueira Province, or continent-continent;
- intraplate models, where the predominant regime is crustal extension.

The Anta Granite and sampling

Anta granite is a small body with dimensions around 2×7 km (~ 14 km²) and is elongated with major axis in the NE-SW direction (Fig. 1B) parallel with the preferential trend of the Paraíba do Sul shear zone. It is intrusive in the paraderivated sequences of the Paraíba do Sul Complex and Rio Turvo suite described by Tupinambá (2012a, 2012b). The pluton is located near the region of the Sapucaia city, Rio de Janeiro State, approximately 1 km from the eastern margin of the main axis of the Paraíba do Sul shear zone. It has features such as “sugarloaf mountain shape”, which is typical of the granitoids from the Ribeira belt. The pluton was initially described by Pinto (1980) and Corrêa Neto *et al.* (1993), who considered it as clearly conditioned by the Paraíba do Sul shear zone

and was classified as collisional (Corrêa Neto *et al.* 1994). However, some authors have classified the body as post-tectonic (Silva *et al.* 2000). Anta granite was not included in the classification of Neoproterozoic granitoids from the Ribeira belt in Rio de Janeiro State, in pre-, syn-, and post-tectonics proposed by Machado and Demange (1994) due to the lack of knowledge on its emplacement since the central portion of the body, apparently macroscopically isotropic, which is not true, as will be shown by magnetic fabrics.

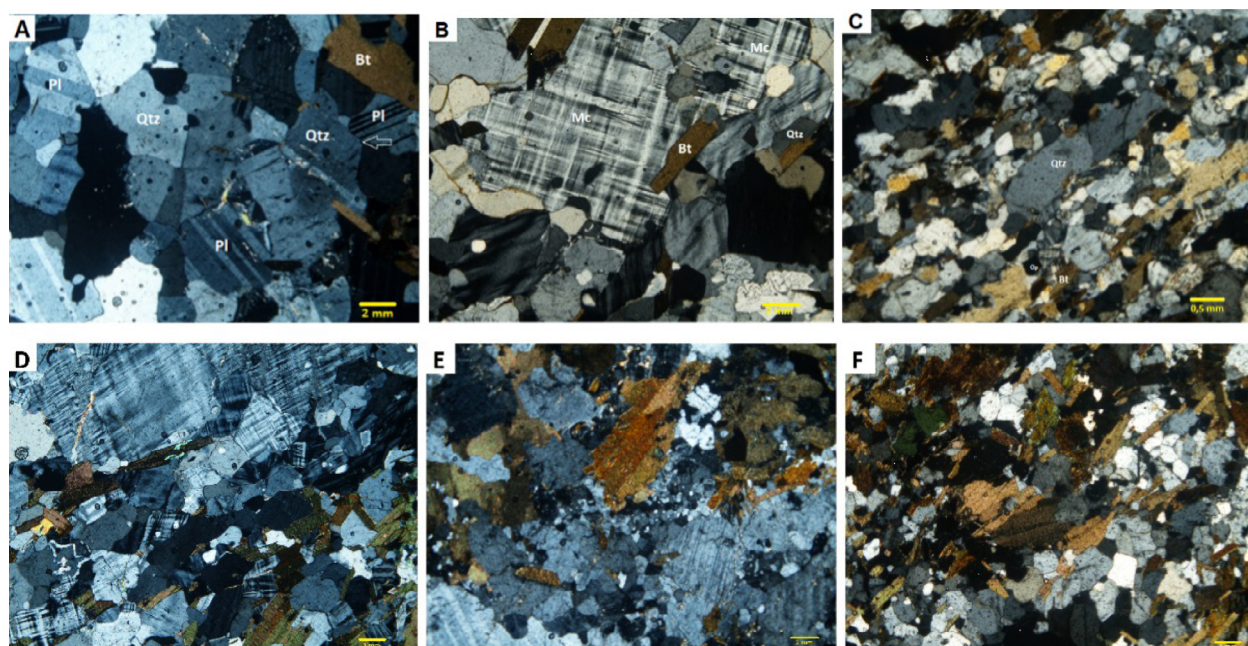
Three distinct facies were identified in the Anta pluton (Fig. 1B). They are:

- more mafic facies composed of hornblende-biotite granodiorite partially foliated to quartz diorite in the eastern portion (SE-NE) of the body;
- an undeformed facies in the center of the pluton (represented here by sites located to SW, AT-10 to AT-14, Fig. 1B) composed of monzogranite and syenogranite;
- a more felsic facies composed of syenogranite to alkali-granite with megacrystal of elongated microcline in the western portion (NW-SW) of the body.

The pluton is deformed at the edges with ENE-WSW-oriented foliation. Lithologically, it is composed of granodiorite, monzodiorite, quartz-diorite, syenogranite, and monzogranite. The different lithologies show different shades of gray and present medium to coarse grains. They have feldspathic porphyroclasts and fractured feldspathic grain lenses, constituting 25 to 75% of the volume, in incipient or advanced recrystallization granoblastic matrix, whose tabular and/or prismatic mafic minerals are oriented according to cataclastic foliation. Petrographic analyses (Fig. 2) show that the essential

mineralogy of granite consists of microcline, orthoclase, quartz, plagioclase, biotite, and hornblende; oxides (mainly titanomagnetites), alanite, and epidote appear as accessories.

In the thin sections (Fig. 2), typical igneous structures are preserved for the lithotypes of the central facies of the Anta granite (Fig. 1B) were observed, such as granoblastic texture and polygonal contacts, slightly deformed at the grain edges (Figs. 2A and 2D). The southwest and west (Fig. 1B, western) facies of the granite show porphyritic texture with microcline megacrystals, sometimes quartz and subordinate plagioclase (Figs. 2B and 2E) that represent relic igneous structures of intergrowth and were formed by processes of static crystallization from a liquid whose original shape may have been modified by deformation. These phenocrysts exhibit undulating extinction levels, brittle/ductile state deformation, and sometimes recrystallized edges surrounded by the mylonitic/protomylonitic matrix. The facies of the northeast border (Fig. 1B, eastern) are composed of predominantly mesocratic quartz, plagioclase, pyroxene, biotite, and hornblende, and were classified as granodiorite and monzodiorite. In this portion of the pluton, mafic bands commonly occur as fine-grained quartz-diorite. This facies presents a higher degree of deformation (Figs. 2C and 2F), with a mylonitic texture, where quartz grains are anhedral and rotate with ribbons formation. The average particle size of the matrix ranges from 0.5 to 5 mm and sub-grain clusters reach up to 15 mm, forming polygonized contacts with plagioclase crystals, suggesting static recrystallization under high-temperature conditions. The plagioclase of these rocks presents an anhedral to subeuhedral shape ranging from medium to coarse granulation (3 to 7 mm), with corroded contacts between the



Pl: plagioclase; Qtz: quartz; Bt: biotite; Mc: microcline.

Figure 2. Photomicrographs, with crossed and plane polarizers light: (A and D) magmatic fabric-coarse-grained monzogranite slightly deformed with polygonal crystals and granoblastic texture (site AT-11, monzo to syenogranite facies), (B and E) sub-magmatic fabric-syenogranite with phenocrystal microcline (site AT-17, porphyritic syenogranite facies) in both (A and B) the igneous textures are still preserved, (C and F) monzodiorite with solid-state deformation in site AT-7 (granodiorite to monzodiorite facies), the quartz ribbons indicate high temperature deformation in this facies.

grains. Biotite has fine to medium granulation and is abundant in the matrix. The rocks of this facies, which have the highest deformation, generally have undulating extinction, grain edge migration, subgrains formation, and even maclas deformation, indicating temperatures between 650–700°C for quartz deformation (Stipp *et al.* 2002).

Geochemical data show that the rocks that make up the Anta granite have expanded composition in the calc-alkaline series, with a predominance of rocks with high SiO₂ content (Tab. 1), as well as with intermediate and basic compositions. These rocks were classified as metalluminous to slightly peraluminous granitoids (Fig. 3A), with remarkable litho-chemical

Table 1. Geochemical data for Anta granite*.

	AT-3	AT-4	AT-12	AT-13	AT-17	AT-18	AT-19	AT-20	AT-21	AT-22
SiO ₂	73.28	50.97	52.05	69.36	68.62	61.92	67.54	75.91	68.68	50.05
TiO ₂	0.229	1.421	1.39	0.345	0.321	0.506	0.577	0.134	0.266	1.730
Al ₂ O ₃	13.76	20.20	19.22	15.18	15.48	18.50	15.28	12.74	15.54	19.79
Fe ₂ O ₃	1.590	8.840	8.270	2.680	2.580	3.370	4.100	1.200	1.770	9.810
MnO	0.02	0.12	0.14	0.05	0.05	0.06	0.07	0.03	0.03	0.14
MgO	0.32	2.75	2.53	0.42	0.35	0.52	0.82	0.08	0.47	3.08
CaO	1.000	6.950	6.100	2.590	1.780	2.090	3.200	0.980	1.500	7.050
Na ₂ O	2.66	4.21	3.91	3.10	2.83	3.83	3.39	2.75	2.92	3.91
K ₂ O	6.04	2.73	3.72	4.92	6.70	7.78	3.48	5.31	7.13	2.90
P ₂ O ₅	0.09	0.48	0.47	0.09	0.08	0.10	0.17	0.02	0.24	0.57
LoI	0.32	0.47	0.40	0.32	0.48	0.33	0.71	0.81	0.53	0.48
Total	99.30	99.14	98.19	99.05	99.26	99.01	99.33	99.96	99.07	99.51
Ba	566	3,361	3,573	1,429	971	731	1160	365	1388	3,511
Ce	138	116	156	110	388	523	127	56	89	126
Cu	6	11	10	5	6	< 5	5	7	9	10
Ga	17	23	23	20	20	19	21	16	19	24
La	57	54	85	73	152	289	75	38	67	56
Nb	< 9	< 9	< 9	10	< 9	< 9	14	< 9	< 9	< 9
Nd	58	60	70	44	110	179	70	20	40	60
Ni	< 5	10	8	< 5	< 5	< 5	< 5	< 5	< 5	10
Pb	37	14	13	16	23	19	13	14	30	10
Rb	180	53	95	188	228	131	111	134	191	65
Sr	107	1,053	884	246	190	168	323	71	515	865
Th	43	7	8	10	24	25	< 7	<	< 7	7
U	6	7	7	5	6	6	5	5	6	7
V	< 9	118	107	15	15	9	38	3	32	142
Y	37	25	26	32	31	25	36	8	18	28
Zn	32	106	112	50	45	60	71	23	30	118
Zr	177	751	686	229	396	701	299	154	106	815
F	74	1,612	1,434	1,047	706	163	806	-1	471	1,885

*Major (%) and trace elements (ppm) concentration of whole rock samples of Anta Granite.

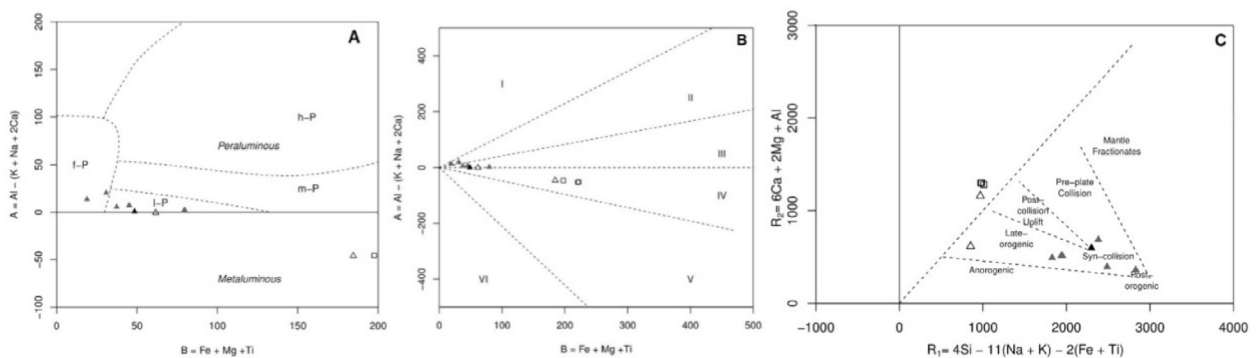


Figure 3. Geochemical diagrams (A) Shand diagram (BA) modified by Villaseca *et al.* (1998): h-P (highly peraluminous) m-P (moderately peraluminous), l-P (low peraluminous), f-P (felsic peraluminous), (B) BA diagram modified by Debon and Le Fort (1983); Fields: I) muscovite > biotite, II) biotite > muscovite, III) biotite, IV) hornblend + biotite, V) Cpx + titanite + epidote, (C) Tectonic classification R1-R2 diagram modified by Batchelor and Bowden (1985).

variation of edge-core transition, in a fractional crystallization system, including rocks of the central portion of the pluton with incipient zonation to the facies recrystallized by metamorphism, as in the eastern portion of the body, with predominance of mafic minerals such as biotite, hornblende, and magnetite, indicating crystallization in medium to deep crust (Fig. 3B). In terms of tectonic environments, the analyzed samples are predominantly distributed in the field of syn-collisional granites; however, some of them fall into the field of late-collisional granites (Fig. 3C).

Oriented samples from 21 sites widely distributed throughout the Anta granite (Fig. 1B) were collected along road cuts and farms in and around Sapucaia city from outcrops, which are certainly *in situ*. Unfortunately, it was not possible to obtain the same site numbers for each facies of equal distributions of the pluton due to the lack of the good outcrop exposure. In some places, large outcrops do occur; however, they are either not *in situ* boulders or are weathered. In addition, we have problems with the access to the higher outcrops, since the Anta granite has “sugarloaf mountain shape.” In spite of this, a significant portion of the Anta pluton could be sampled. Sample orientations were determined using both magnetic and sun compasses, whenever possible. At least 10–13 cores, using a gasoline-powered rock drill, were collected from each site for magnetic measurements, and at least 3 specimens (2.5×2.2 cm) were cut from each core.

MAGNETIC MEASUREMENTS: METHODS

Anisotropy of low-field magnetic susceptibility

The AMS describes the variation of magnetic susceptibility (K) with direction within a rock and represents the contribution of all the rock-forming minerals (*i.e.*, dia-, para-, and ferromagnetic). Its use is not restricted to iron oxide bearing rocks. For anisotropic rocks, K is a symmetrical second-rank tensor which relates the intensity of the applied field (H) to the acquired induced magnetization (M) of a material (Tarling and Hrouda 1993). The tensor is expressed by its principal eigenvalues and eigenvectors $K_{\max} > K_{\text{int}} > K_{\min}$ representing the maximum, intermediate, and minimum axes of susceptibility, respectively. K_{\max} axis represents the magnetic lineation while K_{\min} is the pole of the magnetic foliation (the plane formed by K_{\max} and K_{int} axes). If K AMS is carried by either Fe-bearing silicate paramagnetic matrix minerals or (titano) hematite or pyrrhotite, the AMS, their anisotropy, is due to the preferred mineral crystallographic orientations (magnetocrystalline anisotropy). Otherwise, if K AMS is carried by cubic ferrimagnetic minerals such as titanomagnetite or magnetite, AMS anisotropy is due to the grain shape (shape-anisotropy), in which K_{\max} is parallel to the long axis of the particle (for MD grains), and to the magnetic grain interaction or distribution within a rock. Cañón-Tapia (2001) and Gaillot *et al.* (2006) showed that the AMS might still be dominated by the shape effect, despite the occurrence of magnetic grain interaction or distribution anisotropy in the rock.

AMS data have been used to study a wide variety of geological processes that give a fabric to a rock unit (for reviews, see Borradaile and Henry 1997, Martín-Hernández *et al.* 2004, Herro-Bervera 2006, Martín-Hernández *et al.* 2009; and Almqvist *et al.* 2014). In granite rocks, AMS became widely used, since it is not restricted to remanence-bearing minerals and it can be determined even in rocks with predominant paramagnetic minerals (see the reviews, and Bouchez 1997).

Rock magnetism properties

K-T curves from low-temperature (from about -195°C to room temperature) susceptibility were recorded using a CS3-L apparatus coupled to a Kappabridge (KLY-4S) instrument (Agico, Czech Republic). Specimens were cooled in the Ni N_2 liquid temperature and heated up to room temperature. Corresponding high K-T curves were carried out in an Ar atmosphere using a CS-3 apparatus coupled to the KLY-4S. Specimens were progressively heated up to 700°C and subsequently cooled to room temperature. These experiments were performed on at least one sample from each facies of the granite.

The behavior of NRM was studied by alternate field (AF) tumbling demagnetization in steps of 5 or 10 mT up to 100 mT, this experiment was performed in 12 samples from the distinct facies. All remanences were measured with a JR5A magnetometer (Agico, Czech Republic).

Coercivity remanent spectra from partial anhysteretic remanent magnetization (pARM, Jackson *et al.* 1989) were determined in the same specimens submitted to AF of NRM. They were determined using a Molspin alternating field demagnetizer as the source of the AF field; superimposition of a steady field (DC field) was attained by a small coil (home-made) inside and coaxial to the demagnetizer and it was controlled by a Molspin apparatus. The pARM acquisition consists of applying a steady field (DC field) in between two chosen values (AF window, H_1 and H_2 , $H_1 < H_2$) of a decaying AF peak (H) while the rest of the assemblage is demagnetized from a peak field $H > H_2$. Then, specimens were exposed to an AF peak of 100 mT and DC field of 0.16 mT with an AF window width of 10 mT. Tumbling AF demagnetization at 130 mT was applied after each pARM acquisition.

After AF tumbling demagnetization of the last pARM acquisition, the specimens were subjected to isothermal remanent magnetization (IRM) in progressively increasing magnetizing fields using a pulse magnetometer (MMPM9, Magnetic Measurements).

Hysteresis measurements at room temperature were performed using a vibrating sample magnetometer (VSM-Nuvo, Molspin, Newcastle-upon-Tyne, UK) in fields up to 1 T.

All magnetic measurements were performed at the Laboratory of Magnetic Anisotropies and Rock Magnetism of the Geosciences Institute of the University of São Paulo.

Anisotropy of anhysteretic remanent magnetization

The anisotropy of remanent magnetization isolates the contribution of remanence-bearing minerals from that of

paramagnetic and/or diamagnetic matrix (see Jackson 1991 for a review). This anisotropy is determined from the intensity of an artificial magnetic remanence acquired when a magnetic field is applied along different directions (positions) through the sample. This has distinct advantages because it precludes the effect of inverse AMS fabric due to single domain (SD) titanomagnetite or magnetite (Stephenson *et al.* 1986), since the magnetization occurs always parallel to the long axis of the magnetic grains (Jackson 1991). Among the artificial remanences that can be used to calculate the anisotropy of remanent magnetization tensors, the anhysteretic remanence (AARM) is the most used one, being preferable due to its being acquired in a weak field, which guarantees that the magnetization is linearly related to the inducing field and the AARM tensors are of second-rank. The AARM tensor, as well as AMS, is a symmetrical second-rank tensor expressed by its main eigenvectors $AARM_{max} > AARM_{int} > AARM_{min}$ representing the maximum, intermediate, and minimum axes of anhysteretic remanence intensity, respectively, in which $AARM_{max}$ corresponds to the magnetic lineation and the $AARM_{min}$ is the magnetic foliation pole (normal to $AARM_{max}$ – $AARM_{int}$ plane). Even though less used, the AARM technique has been employed for a wide range of applications in geosciences, such as petrofabric determinations (Trindade *et al.* 1999, Borradaile and Gauthier 2003, Raposo and Gastal 2009, Raposo *et al.* 2012, among others).

The AARM was determined in five sites of the different facies of the Anta granite, in seven positions measurement scheme. The procedure consists of cycles of anhysteretic remanence acquisition, measurement, and demagnetization along different positions for each specimen. The AARM tensor was determined by iteratively magnetizing the specimen in an AF peak of 60 mT (this field was chosen based on the coercivity remanent spectra) with a DC field of 0.16 mT in the desired orientation, measuring the resulting remanence, and AF tumble-demagnetizing in 120 mT before proceeding to the next step. Before AARM determinations, the samples were demagnetized by AF tumbling at 200 mT to establish the base level. The best-fit AARM tensors were calculated by the least-squares method, which showed root-mean-squares of less than 5%, indicating that the ellipsoids are well-resolved (Jackson 1991).

MAGNETIC MEASUREMENTS: RESULTS

Anisotropy of low-field magnetic susceptibility directional and scalar data

AMS measurements were performed on 2.5×2.2 cm cylindrical specimens that were cut from the cores collected from 22 sites of the Anta pluton, using a Kappabridge instrument (KLY-4S, Agico, Czech Republic). The mean AMS eigenvectors (K_{max} , K_{int} , K_{min}) and the 95% confidence regions for each site were calculated using the ANISOFT 4.2 (Agico, Czech Republic). Scalar and directional AMS data are presented in Table 2.

The eigenvectors within the sites are generally well grouped with low values and small angles for the 95% confidence

regions (Tab. 2) as observed in the representative examples of the Figure 4. For the majority of the sites, the magnetic lineation (K_{max}) is NE/SW oriented (Figs. 4A and 4D) with a slight variation to E/W (Figs. 4B, 4C and 4F), the plunges range from horizontal ($< 20^\circ$, Figs. 4A and 4D) to inclined moderate inclination (between 20 and 40°), the most inclined plunge ($> 60^\circ$) was found only in one site AT-11 (Fig. 4E, Tab. 2). The magnetic foliations (K_{max} – K_{int} plane) are preferably NE/SW oriented with dips from horizontal to vertical (Fig. 4). Both magnetic lineations and foliations are, in part, similar to the lineations and foliations measured in the Paraíba do Sul shear zone.

The mean magnetic susceptibility, expressed by the arithmetic average of $K_m = (K_{max} + K_{int} + K_{min})/3$ in SI units, is generally high for all facies (Tab. 2), ranging from 0.25×10^{-3} (AT-14) to 96.07×10^{-3} (AT-4) with an average of 26.19×10^{-3} . High and low values of K_m are found in the borders and central part of the pluton.

The mean of the degree of anisotropy, given by the arithmetic average of $P = K_{max}/K_{min}$, ranging from 1.08 (8%, AT-19) to 2.22 (122%, AT-8, Tab. 2) with an average of 1.40 (40%). Even though P values are variables between the lithological units, the highest values are in the borders of the pluton, mainly in the deformed mafic units (granodiorite to monzodiorite)

In general, there is no clear relation between K_m and P parameters for the Anta granite facies (Fig. 5A). The Jelinek's (1981) shape parameter of the ellipsoid expressed by $T = [2\ln(K_{int}/K_{min})/\ln(K_{max}/K_{min})] - 1$ is oblate ($T > 0$) and triaxial ($T \sim 0$) for the majority of sites (Tab. 2, Fig. 5B); however, for few sites, it is prolate ($T < 0$, Fig. 5B).

Rock magnetism properties

Representative examples of K-T curves are shown in Fig. 6A for different facies of the Anta granite. In all analyzed specimens, a well-defined peak was observed around -150°C , which indicates the Verwey transition, characteristic of almost pure magnetite. The correspondent high K-T curves show a small Hopkinson peak, and all of them display a decrease in the intensity of susceptibility around 580°C (Fig. 6A), indicating the presence of Ti-poor titanomagnetite or magnetite. The cooling and heating curves are reversible.

Examples of acquisition of remanent coercivity spectra determined from AF demagnetization of natural remanent magnetization (NRM) are shown in Figure 6B. The remanent coercivity is generally low, with medium destructive field < 20 mT, characteristic of multi-domain magnetite grains.

Results from the pARM curves are presented in Figure 6C, which show that all samples are of low coercivity, indicating that magnetite grains are relatively large around 2 – $5 \mu\text{m}$, since coercivity is linked to grain size (Jackson *et al.* 1989).

The IRM pattern is shown in Figure 6D, which displays that more than 95% of the magnetization reaches the total saturated isothermal remanent magnetization (SIRM) in fields < 150 mT, except for two samples (AT-17 and AT-18) whose total saturation is reached in fields < 200 – 250 mT (Fig. 6D). The IRM curves indicate the presence of fully saturated, coarse

Table 2. Anisotropy of low-field magnetic susceptibility (AMS) data for Anta granite.

Site	Latitude	Longitude	Unit	N	NRM	Mean AMS parameters				Mean AMS eigenvectors						
						Km (10 ⁻³)	L	F	P	T	Kmax dec/incl	e/z	Kint dec/incl	e/z	Kmin dec/incl	e/z
AT1	-22°01'57.2"	-42°56'10.5"	OGN	49	2.09	1.07	1.23	1.32	1.50	0.50	141/37	65/14	181/46	65/10	166/13	15/10
AT3	-22°00'48.8"	-42°56'04.4"	MGT	33	0.31	1.04	1.11	1.15	0.51	0.51	68/26	19/13	209/60	18/8	290/12	16/7
AT4	-22°01'49.5"	-42°56'14.3"	GDT	41	96.07	1.10	1.15	1.26	0.17	0.17	90/31	20/8	257/41	24/9	204/33	23/7
AT5	-22°01'43.5"	-42°56'11.2"	GDT	40	57.08	1.05	1.05	1.11	-0.02	-0.02	190/40	29/11	181/21	42/13	165/37	41/7
AT6	-22°01'34.6"	-42°56'04.1"	GDT	34	5.95	1.63	1.20	1.95	-0.47	-0.47	102/16	15/7	196/63	21/15	297/18	21/8
AT7	-22°01'34.0"	-42°55'59.6"	GDT	35	24.99	1.36	1.28	1.75	-0.08	-0.08	112/16	12/8	202/68	14/11	272/12	15/8
AT8	-22°01'10.8"	-42°55'40.5"	GDT	38	53.39	1.91	1.16	2.22	-0.63	-0.63	54/12	13/4	162/57	27/11	301/29	27/8
AT9	-22°00'58.5"	-42°55'39.2"	GDT	33	26.33	1.50	1.17	1.76	-0.44	-0.44	33/23	10/2	182/61	13/6	274/15	13/9
AT10	-22°02'13.4"	-42°57'08.7"	MGT	32	43.84	1.09	1.09	1.19	0.04	0.04	86/14	10/6	167/28	12/8	298/58	13/7
AT11	-22°02'10.4"	-42°57'18.0"	MGT	28	42.62	1.12	1.13	1.27	-0.02	-0.02	206/62	24/10	158/17	24/22	133/19	22/11
AT12	-22°02'18.8"	-42°57'37.3"	MGT	42	90.86	1.10	1.19	1.31	0.31	0.31	230/7	10/4	160/20	11/6	180/69	7/5
AT13	-22°02'19.7"	-42°57'40.2"	MGT	38	5.93	1.08	1.23	1.33	0.48	0.48	104/22	75/11	155/18	75/16	273/58	18/11
AT14	-22°02'06.4"	-42°57'59.7"	MGT	40	0.25	1.05	1.08	1.13	0.26	0.26	62/30	10/7	260/57	10/8	159/12	8/6
AT15	-22°00'48.9"	-42°56'15.1"	SGP	36	4.34	1.13	1.14	1.29	0.13	0.13	99/40	22/12	219/45	22/16	237/13	17/14
AT16	-22°00'52.9"	-42°56'22.2"	MGT	36	4.32	1.23	1.19	1.46	-0.13	-0.13	86/16	16/10	185/61	13/8	320/20	16/11
AT17	-22°02'54.2"	-42°57'39.8"	SGP	33	0.02	1.08	1.17	1.27	0.33	0.33	111/24	34/13	236/17	34/16	194/57	17/11
AT18	-22°01'21.6"	-42°57'07.9"	SGP	40	0.15	1.16	1.09	1.26	-0.22	-0.22	112/40	14/8	179/32	73/11	260/28	72/10
AT19	-22°01'33.6"	-42°57'13.9"	MGT	25	0.50	1.03	1.05	1.08	0.25	0.25	125/20	67/15	133/23	67/16	279/54	16/15
AT20	-22°01'07.1"	-42°56'54.1"	SGP	35	7.96	1.18	1.15	1.36	-0.03	-0.03	96/30	11/8	207/35	17/8	281/38	18/8
AT21	-22°02'21.3"	-42°56'26.1"	OGN	34	6.72	1.22	1.29	1.57	0.11	0.11	83/15	14/10	275/52	16/8	143/32	12/10
AT22	-22°01'51.3"	-42°56'30.5"	GDT	35	82.64	1.28	1.13	1.45	-0.26	-0.26	54/24	20/7	233/43	51/15	253/34	50/8
Mean:					26.85	1.21	1.16	1.40	0.04	0.04						

Unit: the lithological facies; ogn: orthogneiss (countryrock); mgt: monzogranite; gdt: granodiorite; sgp: syenogranite; N: the number of specimens included in the AMS means; K_m: the mean magnetic susceptibility (SI units); P: the degree of anisotropy; T: the Jelinek's shape parameter (Jelinek 1981); K_{max}, K_{int} and K_{min}: mean AMS eigenvectors which represent the maximum, intermediate and minimum susceptibility intensities, respectively; Dec: declination in degrees; Inc: inclination in degrees; e/z: the semi angles of the major and minor axes of the 95% confidence ellipse, respectively, calculated by the Jelinek (1981) statistic; NRM: natural remanent magnetization (A/m²).

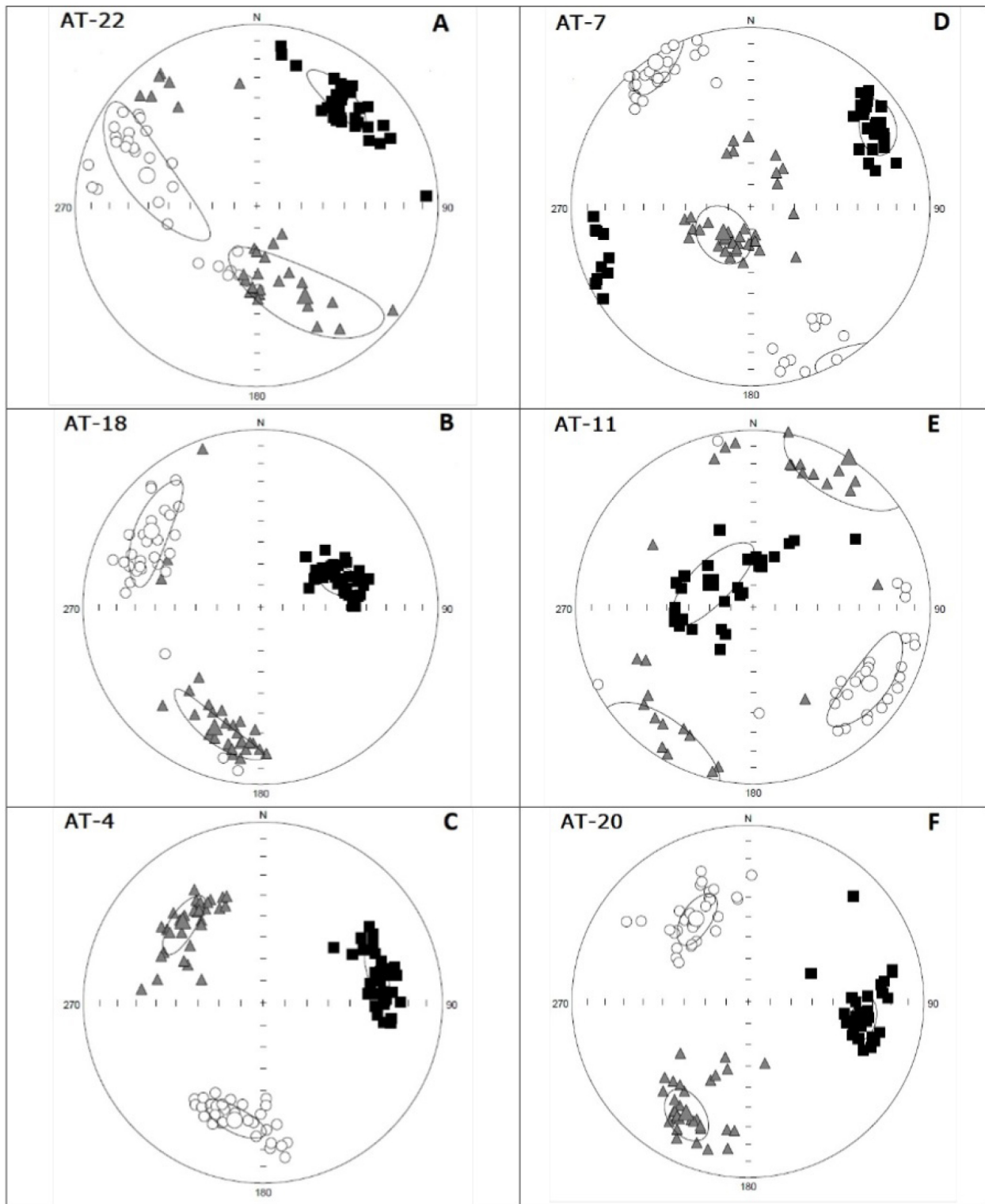


Figure 4. Representative examples of anisotropy of low-field magnetic susceptibility (AMS) fabrics for Anta pluton. Squares are the maximum susceptibility (K_{max}), triangles are the intermediate susceptibility (K_{int}) and circles are the minimum susceptibility (K_{min}). Dashed line ellipses are the 95% confidence ellipses. Data plotted in the lower hemisphere stereonet.

and fine magnetite grains, which is in agreement with the pARM spectra (Fig. 6C).

Some typical hysteresis curves from the analyzed facies are illustrated in Figure 7. For all units, the shape of the hysteresis curves reveals that ferromagnetic grains carry bulk susceptibility. However, for some specimens, hysteresis loops show that there is a significant contribution (> 80%, Figs. 7B,

7C and 7D) of paramagnetic minerals to the bulk magnetic susceptibility, as can be observed in the high-field part of the hysteresis curves. In general, hysteresis curves for the majority of the specimens (Fig. 7) are narrowing waisted, typical of low-coercivity ferromagnetic grains since the loops are totally closed at 0.2 T. In addition, most samples fall into MD domain state on the Dunlop's (2002) plot (Fig. 7E), which is coherent

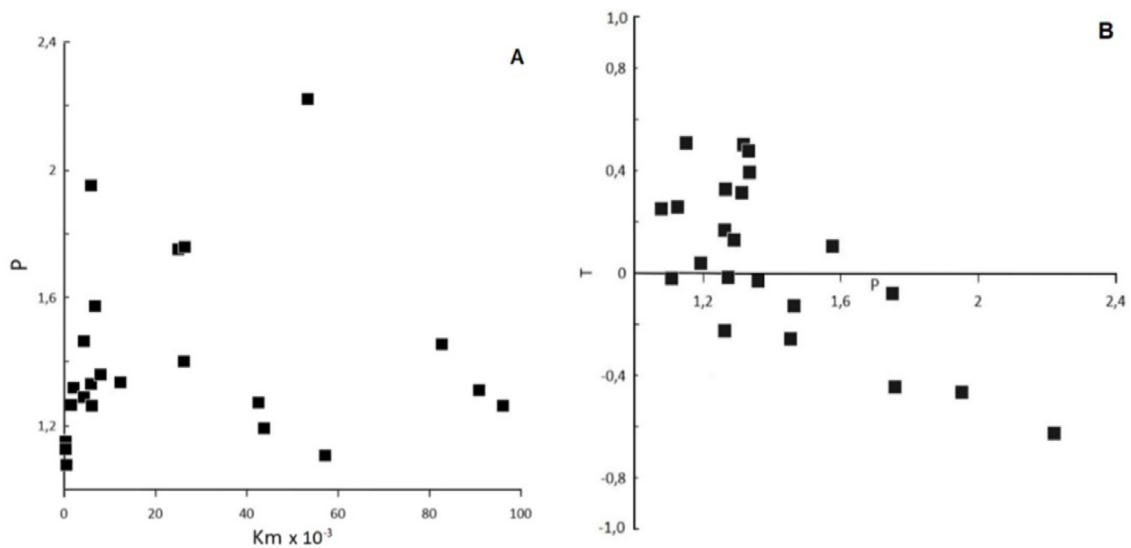


Figure 5. Anisotropy of low-field magnetic susceptibility (AMS) scalar data. (A) K_m vs. P plot; (B) P vs. T plot.

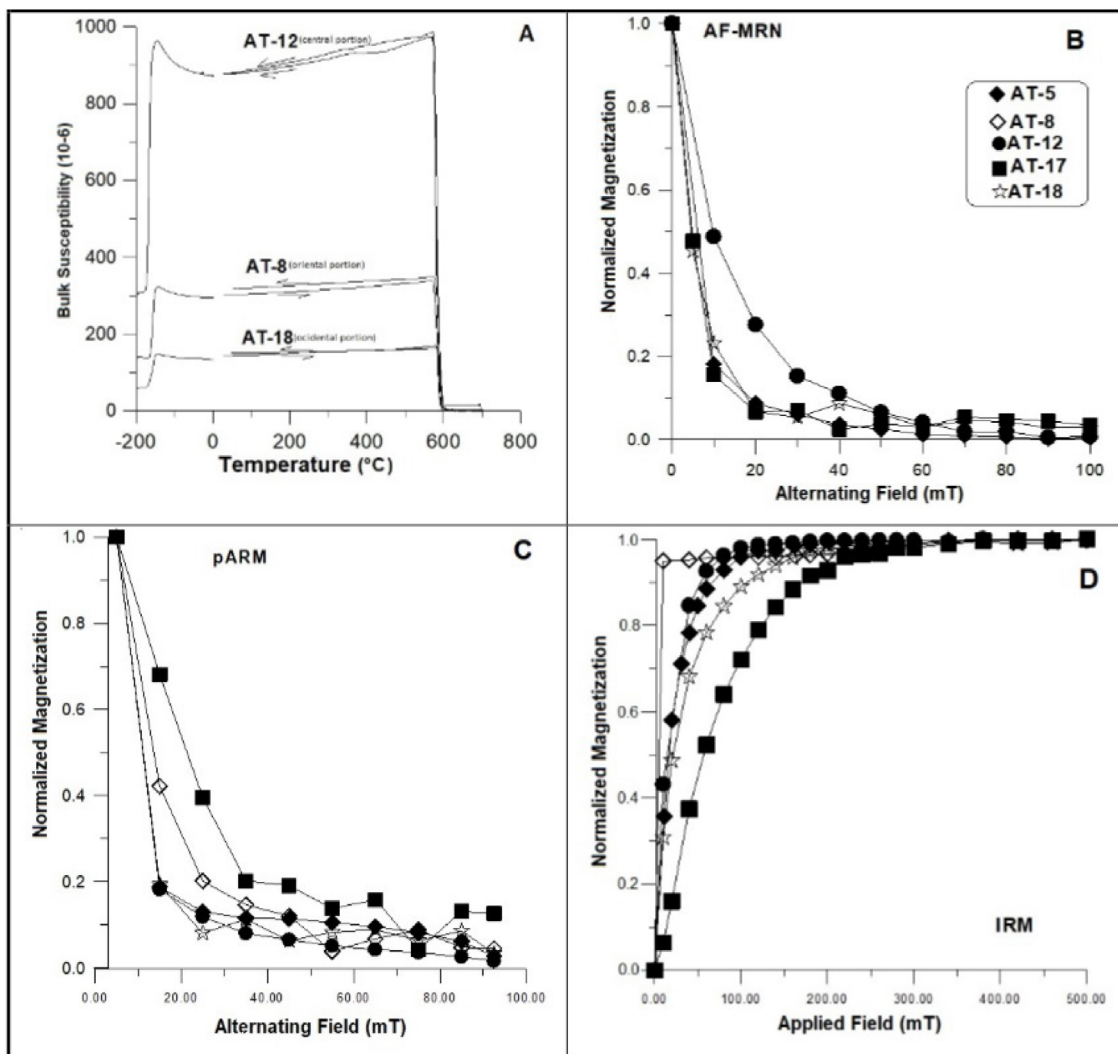


Figure 6. Representative examples of rock magnetism for samples from all studied facies. (A) K-T curves (susceptibility versus low (Ni liquid) and high temperatures obtained in argon atmosphere) (B) Remanent coercivity spectra determined from AF tumbling demagnetization of natural remanent magnetization (NRM). Remanence intensities are normalized to the first measurement; (C) Remanent coercivity spectra derived from partial anhysteretic remanence (pARM) acquisition in an AF peak demagnetization at 100 mT with AF window width of 10 mT during DC field application of 0.16 mT. Remanence intensities are normalized to the highest value of partial remanence acquisition; (D) Isothermal remanence magnetization (IRM) acquisition curves, intensities of remanences are normalized to saturation of IRM (SIRM) versus field strength. AT-5 and AT-8 are from granodiorite to monzodiorite facies, AT-12 and AT-18 are from monzo- to syenogranite facies, and AT-17 is from porphyritic syenogranite facies.

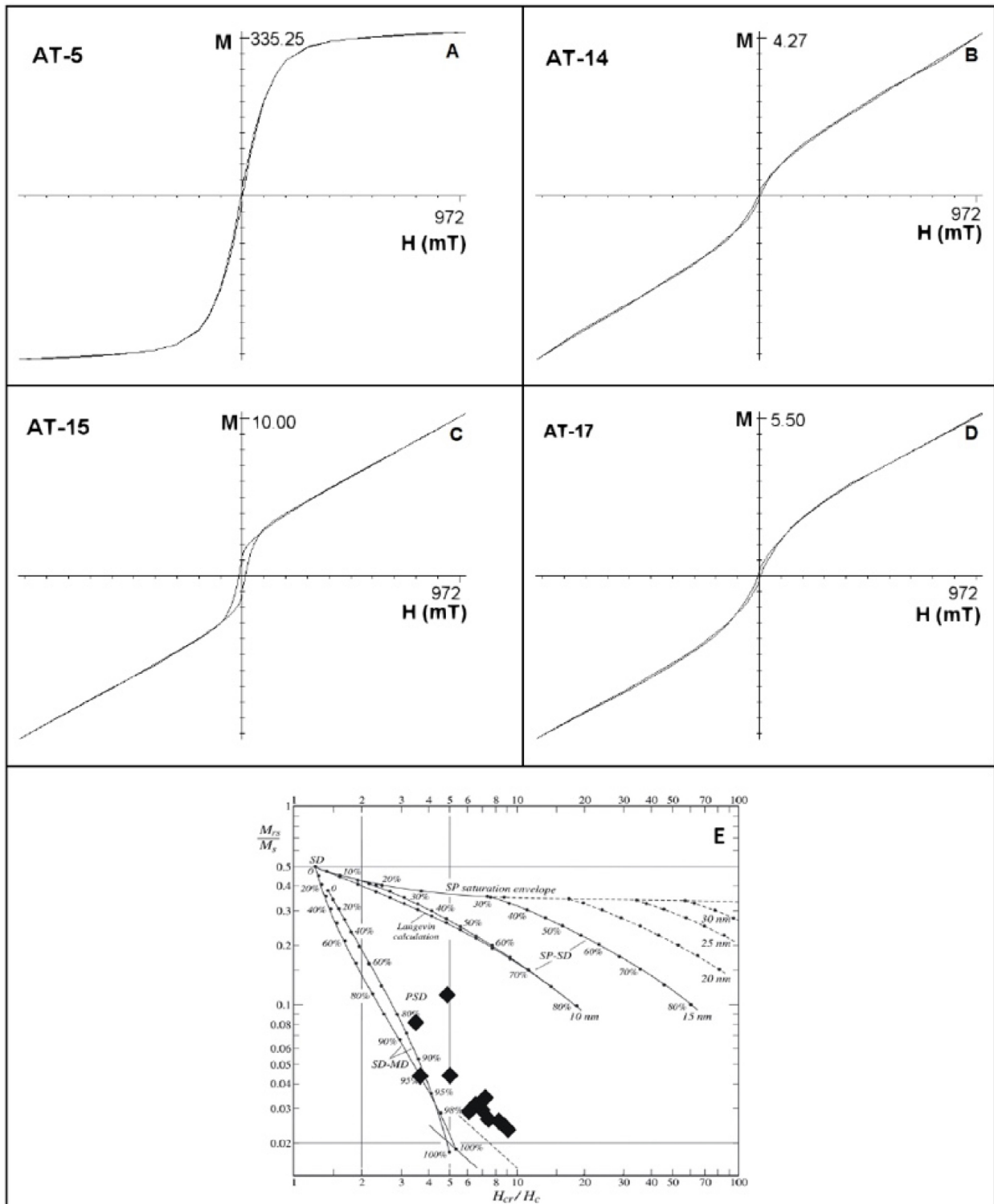


Figure 7. Representative hysteresis loops for samples from Anta pluton. M is magnetization in μAm^2 and H is applied field. Loops are not corrected for paramagnetic slopes. (E) Dunlop's (2002) plot. The contribution for magnetic susceptibility of ferromagnetic (Kfe) and paramagnetic (Kpa) are in percentage from the total, and Hcr = remanent coercivity. For AT-5, Kfe = 99.28, Kpa = 0.72, Hcr = 28.3. For AT-14, Kfe = 77.71, Kpa = 28.29, Hcr = 30.0. For AT-15, Kfe = 89.88, Kpa = 10.12, Hcr = 27.67. For AT-17, Kfe = 81.27, Kpa = 18.73, Hcr = 27.56.

with other experiments such as the IRM and pARM acquisition curves (Figs. 6C and 6D).

Based on all magnetic experiments, therefore, we conclude that coarse magnetite, which was also observed in thin sections, carry NRM and IRM magnetizations and are responsible for magnetic susceptibility, with few or significant contribution (> 80%) of the paramagnetic matrix minerals of the Anta pluton.

Anisotropy of anhysteretic remanent magnetization directional and scalar data

The AARM tensor was obtained in at least 6 specimens from the five sites (Tab. 3). The mean AARM eigenvectors (AARM_{max} , AARM_{int} , AARM_{min}) and the 95% confidence regions for each site were also calculated using the ANISOFT 4.2 (Agico, Czech Republic). In all analyzed sites,

Table 3. Anisotropy of anhysteretic remanent magnetization (AARM) data for Anta Granite.

Site	Unit	N	Mean AARM parameters		Mean AARM eigenvectors					
			P	T	AARM Dec/ Inc (max)	e/z	AARM Dec/ Inc (int)	e/z	AARM Dec/ Inc (min)	e/z
AT9	GDT	6	2.10	-0.73	35/25	11/3	150/41	45/5	283/38	46/8
AT10	MGT	6	1.17	-0.09	67/17	36/16	181/53	38/21	326/22	30/11
AT12	MGT	6	1.29	0.22	252/6	20/7	160/16	19/6	3/73	10/1
AT17	SGP	9	1.45	0.94	90/8	79/7	355/28	79/13	194/61	13/8
AT19	MGT	14	1.15	-0.13	112/14	24/22	206/17	32/24	345/68	32/22
Mean:			1.43	0.04						

Unit: the lithological facies; N: the number of measured specimens; P: the degree of anisotropy; T: the Jelinek's shape parameter (Jelinek 1981); $AARM_{max}$, $AARM_{int}$ and $AARM_{min}$: mean AARM eigenvectors which represent the maximum, intermediate and minimum remanent magnetization intensities, respectively; Dec: declination in degrees; Inc: inclination in degrees; e/z: the semi angles of the major and minor axes of the 95% confidence ellipse, respectively, calculated by the Jelinek (1981) statistic.

AARM and AMS tensors are coaxial, as observed in the representative examples showed in Figure 8. This means that if fine SD magnetite grains are present, they did not affect the AMS fabrics. Therefore, the AMS fabrics of the Anta granite are normal ones, *i.e.*, the magnetic fabric is similar to the petrofabric. In addition, both magnetite grains and paramagnetic matrix minerals of the Anta pluton have the same orientation.

DISCUSSION

The magnetic fabric patterns in the Anta pluton are presented in Figures 9 (foliations) and 10 (lineations). Magnetic foliations (normal to K_{min} , Fig. 9) are roughly parallel to the foliation measured in the field in the country rocks in a regional scale (inset, Fig. 9). They are predominantly NE-SW oriented with steeply dipping or vertical in all units (Fig. 9) for the majority of sites. It is worth noting that the sites with the highest foliation dips are located in the borders portion of the pluton (Fig. 9), where the pluton is solid-state deformed (Fig. 2).

Magnetic lineations, K_{max} (Fig. 10), are mainly ENE oriented and present mostly low plunges ($< 30^\circ$) in approximately 85% of the sites, again most of them located at the border portion of the pluton; however, in some sites, K_{max} is also ESE oriented (Fig. 10, Tab. 2). Seven sites display magnetic lineation plunges between 30 and 60° , and in one site, the plunges are $> 60^\circ$, located at central facies of the granite (AT-11, Figs. 1B and 10) where foliation is not observed in the field, and also no solid state deformation was observed even in the thin section (Figs. 2A and 2D), in which the primary magmatic structures are preserved. In general, the pattern of magnetic lineations is roughly measured in the field in the country rocks in a regional scale (inset, Fig. 10).

Fabrics in plutons are regarded either as related to magma emplacement or resulting from tectonic strain after or syn-tectonic. Therefore, fabric patterns in plutons can result from internal magma chamber processes such as magma pulses, convection, magma surges, dike injections, and crystal settling,

or even be related to regional deformation, or involve a combination of these two processes (Paterson *et al.* 1998), which is characteristic of syn-tectonic regimes. However, this combination can be simultaneous, if a compressive component predominates during intrusion; or subsequent, considering that an intimate association of extension and compression is commonly observed along shear zones. In such a case, an originally vertical lineation may be obliterated by the shearing process. Indeed, fabrics related to emplacement such as the presence of magmatic microstructures and steep lineations are rarely preserved, since they are easily overprinted by minor ductile strain during or after cooling of the magma (Clemens *et al.* 1997). These overprinted fabrics may be observed in the whole pluton, or in some places, which is more common.

Comparing oriented structures from country rocks with internal magnetic and deformational fabrics in plutons allows determining whether pluton fabrics reflect the effect of regional tectonic strain. On the other hand, if foliations and lineations in country rocks and pluton are different, structures in the pluton will preferentially be considered as the result of internal processes in the pluton.

Field and petrographic evidence (Fig. 2) show that rocks from the Anta pluton were affected by the regional strain during and after emplacement, since magmatic foliation evolves to solid-state deformation higher in the oriental eastern border (*e.g.*, AT-7 and AT-8, Fig. 2C) than the occidental western border (AT-17) of the pluton (Fig. 2B). Magnetic foliations for these rocks are steeply dipping and parallel to foliation measured in the field (inset, Fig. 9). The lineations are mostly subhorizontal. This indicates that magnetic fabrics in these portions of the pluton record this strain which is related to the dextral Paraiba do Sul shear zone (Fig. 1A), which controlled, in parts, the Anta emplacement. On the other hand, no deformation is observed in rocks from central facies of the pluton (*e.g.*, AT-10, AT-11, AT-12, AT-13, and AT-14, Figs. 1B), the thin section (*e.g.* Figs. 2A and 2D) shows that primary magmatic structures were preserved. In fact, even magmatic foliation observed in the field in these sites and magnetic foliations are not parallel either to magnetic foliations from the eastern and

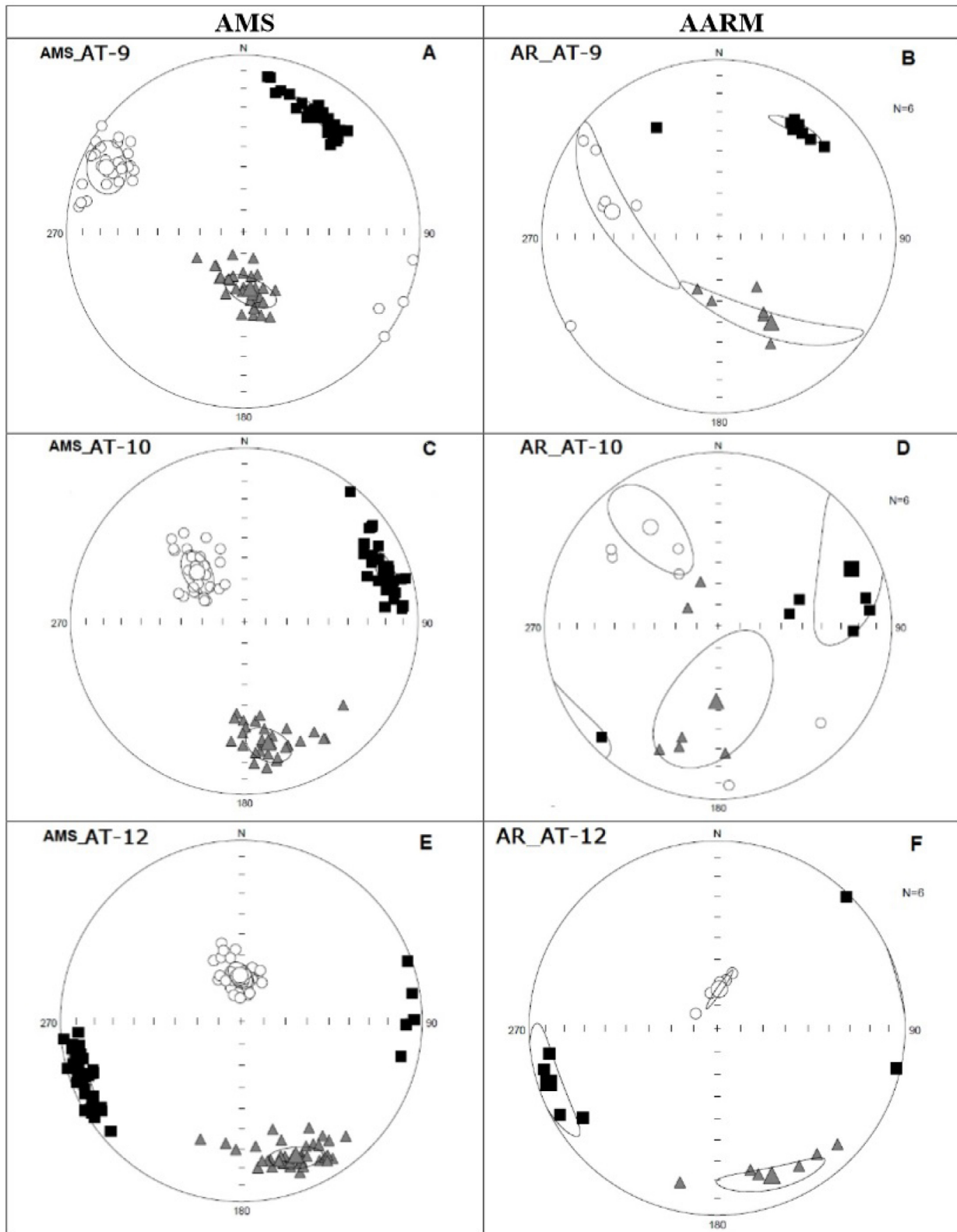


Figure 8. Examples of magnetic fabrics determined from both anisotropy of low-field magnetic susceptibility (AMS) and anisotropy of anhysteretic remanent magnetization (AARM). All magnetic fabrics are coaxial. Squares are maximum susceptibility (K_{max}) and maximum remanence ($AARM_{max}$); triangles are intermediate susceptibility (K_{int}) and intermediate remanence ($AARM_{int}$) and circles are minimum susceptibility (K_{min}) and minimum remanence ($AARM_{min}$). Dashed line ellipses = 95% confidence ellipses. Data plotted in the lower hemisphere stereonets. AT-9 is granodiorite to monzodiorite, AT-10 and AT-12 are monzo- to syenogranite.

western part of the pluton or to the regional deformation pattern (Fig. 9). Also, the magnetic lineation (Fig. 10) plunges from moderately to steeply. This indicates that the central portion of the Anta pluton was not affected by any tectonic deformation either during or after the emplacement, and

magnetic fabric in this part of the pluton is probably primary (magmatic) in origin, acquired when the rocks were solidified reflecting magma flow. Therefore, the highest plunge lineation (AT-11, Figs. 2A and 10) could be linked to a magma feeder zone (magma chamber).

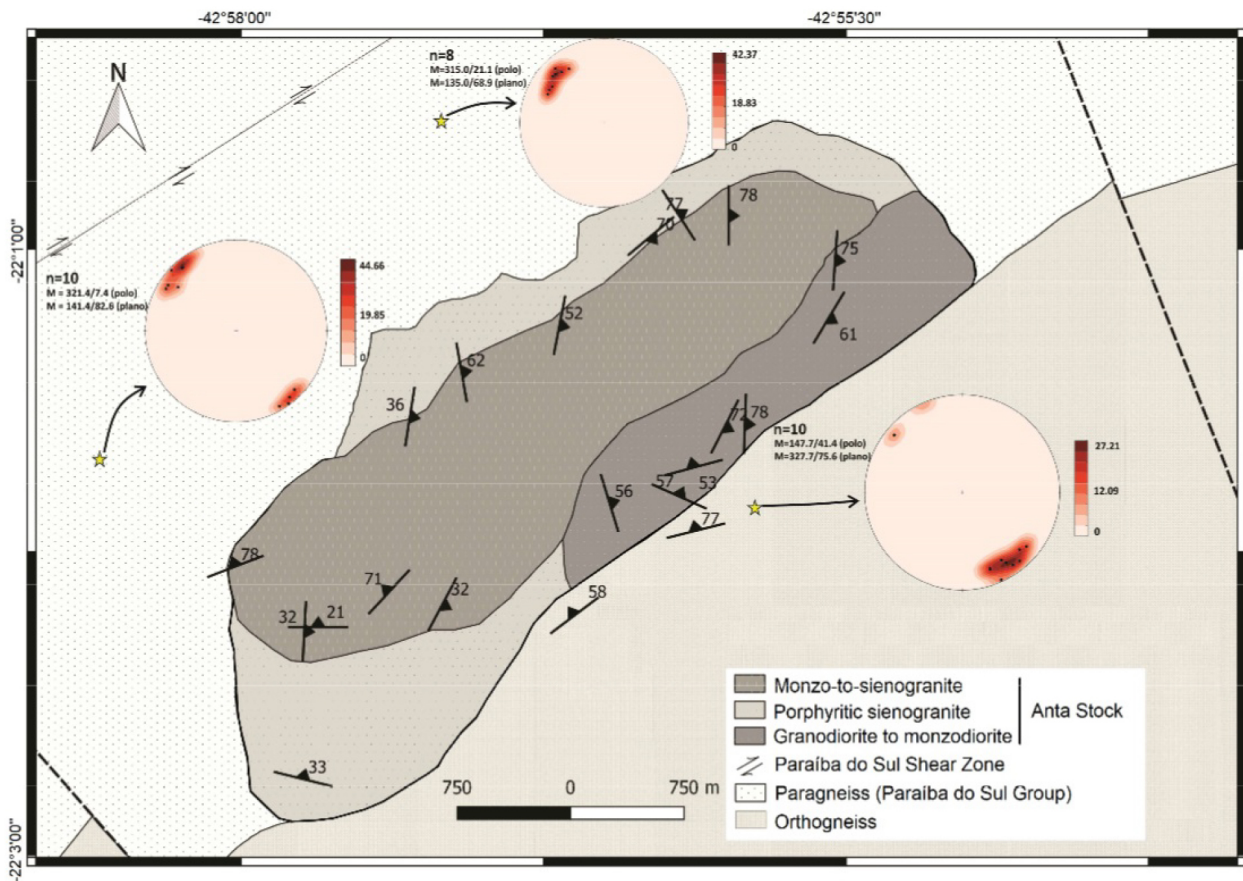


Figure 9. Magnetic foliation (normal to K_{min}) pattern of the Anta pluton. The inset steronets (data plotted in the lower hemisphere) correspond to poles from foliations measured in the field for country rocks.

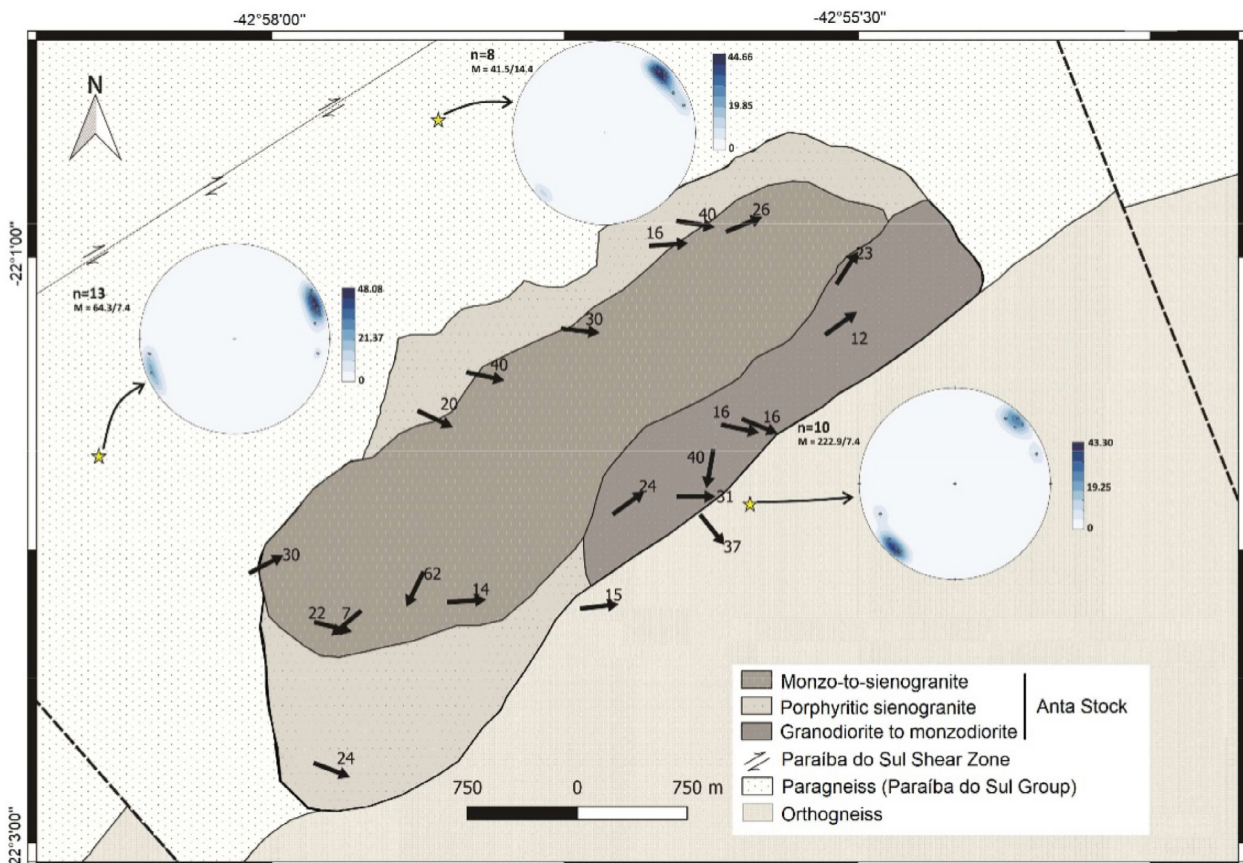
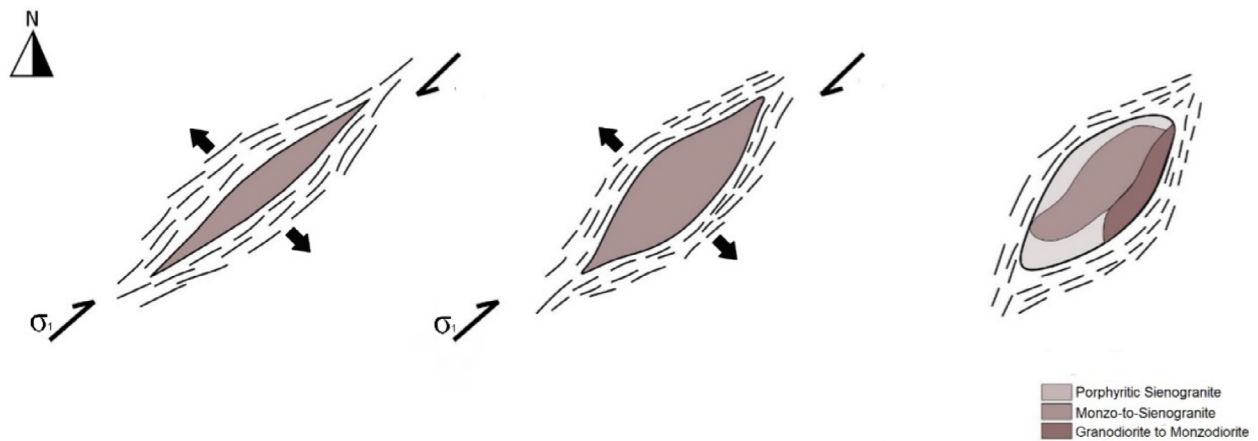


Figure 10. Magnetic lineation (K_{max}) pattern Anta pluton. The inset steronets (data plotted in the lower hemisphere) correspond to the lineations measured in the field for country rocks.



Source: adapted from Bhatt *et al.* (2017).

Figure 11. Dimensional model emplacement in the dextral and transpressional movement for the Anta granite

Since the borders — mainly the eastern one — of the pluton was affected by regional deformation, a question arises on whether the subhorizontal lineation represents an overprint of an initially steep lineation, reworked by shearing during or after emplacement. The AARM results clearly show that there is not a fabric overprint (*i.e.*, AMS and AARM tensors are coaxial, Fig. 8). Two hypotheses can be evoked:

- considering the syn-tectonic character of Anta granite, this regime affected only the borders of the pluton, which means that the magnetic fabric would be tectonic in origin, and the central section would represent an area of extension and, therefore, a preferential place for the ascension of magmas, as has been suggested by Raposo *et al.* (2012) for Piracaia pluton. Due to the dynamics of the Paraíba do Sul shear zone, the magma would be affected by strain and flow toward the borders, acquiring a magmatic foliation which evolved to solid state upon cooling;
- considering that the highest plunge of magnetic lineation points toward south (in the central part of the pluton, AT-11, Fig. 10), it can be reasonably argued that the sites from the western border (which is less deformed) were strained by the shear zone. Low lineation plunges would be showing that these sites were fed by the source in the central portion (SW) of the pluton, in which high lineation plunges are found.

The latter hypothesis is corroborated by other undeformed sites from the central part. If this hypothesis is right, then the magma ascent started from the source in the SW part of the pluton and migrated to the borders, concomitantly with the movement of Paraíba do Sul shear zone that affected (syn-tectonically) this portion of the pluton. Therefore, the emplacement of Anta granite probably occurred during a local transpression due to a weak zone generated by Paraíba do Sul shear zone, in the syn-magmatism orogenic phase that generated the transcurrent and transpressive opening that enabled diapirism with magmatic shortening, enabling the emplacement of the pluton. This weak zone was generated by thrust faults of orogenic

eastern blocks over cratonic western blocks and refolded by Brazilian-Pan African orogeny recorded before to the syn-late magmatism (Heilbron and Machado 2003, Heilbron *et al.* 2013, Machado 2000). After that, the magmatic chamber housed in a transpressive regime, with a distensive component, was crystallized with a fractionated zoning (Fig. 11) similar to a model proposed by Bhatt *et al.* (2017), but in our case, with dextral movement.

SUMMARY AND CONCLUSION

The Anta pluton is composed of five petrographic units. Rock-magnetism determinations have allowed the characterization of magnetic properties and determine the internal fabric of the pluton. No SD effect was found in the AMS fabrics, as showed by rock-magnetism and AARM. The main magnetic mineral are magnetite grains, which are certainly responsible by magnetic susceptibility and AARM and probably by AMS fabric. No SD effect was found in the AMS fabrics, as showed by rock-magnetism, AARM and Dunlop's (2002) plot. The main magnetic mineral are magnetite grains, which are certainly responsible by magnetic susceptibility and AARM and probably by AMS fabric. Therefore, the AMS and AARM in the studied rocks are mainly due to the shape preferred orientation of magnetite grains. Both AMS and AARM tensors are coaxial and partially related to regional strain in the borders of the pluton, whereas they are related to magma flow in the central part (SW) of the pluton, where high lineation plunge suggests that this place could be linked to a magma feeder zone. Our data suggest that the regional strain did not affect the whole pluton.

ACKNOWLEDGMENTS

We thank FAPESP (17/01120-0 grant), Brazilian agency, for its financial support. Odirney Benedito da Silva thanks CNPq (Brazilian agency) for Msc scholarship (134419/2016-2 grant). We also, thank Emilio L. Pueyo and Wentian Liang, whose comments greatly improved the manuscript.

ARTICLE INFORMATION

Manuscript ID: 20200007. Received on: 01/29/2020. Approved on: 07/30/2020.

O.B.S. was responsible for the measurements of rock-magnetism and the model presented in the manuscript, wrote the geological setting, and prepared the Figures and Tables; M.I.B.R. was the advisor, wrote the first and the final versions of the manuscript, and participated in all parts of the manuscript.

Competing interests: The authors declare no competing interests.

REFERENCES

- Almeida F.F.M., Hasui Y., Brito Neves B.B., Fuck R.A. 1981. Brazilian structural provinces: an introduction. *Earth-Science Review*, **17**(1-2):1-29. [https://doi.org/10.1016/0012-8252\(81\)90003-9](https://doi.org/10.1016/0012-8252(81)90003-9)
- Almqvist B.S.G., Henry B., Jackson M., Werner T., Lagroix F. (Eds.). 2014. *Methods and Applications of Magnetic Anisotropy: A Tribute to Graham Borradaile*. Tectonophysics Special Issue. Amsterdam: Elsevier. 377 p.
- Archanjo C.J., Macedo J.W.P., Galindo A.C., Araújo M.G.S. 1998. Brasiliano crustal extension and emplacement fabrics of the mangerite–charnockite pluton of Umarizal, North-east Brazil. *Precambrian Research*, **87**(1-2):19-32. [http://dx.doi.org/10.1016/S0301-9268\(97\)00050-8](http://dx.doi.org/10.1016/S0301-9268(97)00050-8)
- Archanjo C.J., Trindade R.I.F., Bouchez J.L., Ernesto M. 2002. Granite fabrics and regional-scale strain partitioning in the Seridó belt (Borborema Province, NE Brazil): Granite fabrics in the Seridó belt. *Tectonics*, **21**(1):3-14. <https://doi.org/10.1029/2000TC001269>
- Basei M.A.S., Brito Neves B.B., Siga Junior O., Babinski M., Pimentel M.M., Tassinari C.C.G., Hollanda M.H.B., Nutman A., Cordani U.G. 2010. Contribution of SHRIMP UePb zircon geochronology to unravelling the evolution of Brazilian neoproterozoic fold belts. *Precambrian Research*, **183**(1):112-144. <http://dx.doi.org/10.1016/j.precamres.2010.07.015>
- Batchelor R.A., Bowden P. 1985. Petrogenetic Interpretation of Granitoid Rock Series Using Multicationic Parameters. *Chemical Geology*, **48**(1-4):43-55. [https://doi.org/10.1016/0009-2541\(85\)90034-8](https://doi.org/10.1016/0009-2541(85)90034-8)
- Benn K. 1994. Overprinting of magnetic fabrics in granites by small strains: numerical modelling. *Tectonophysics*, **233**(3-4):153-162. [https://doi.org/10.1016/0040-1951\(94\)90238-0](https://doi.org/10.1016/0040-1951(94)90238-0)
- Bento dos Santos T.M., Tassinari C.C.G., Fonseca P.E. 2015. Diachronic collision, slab break-off and long-term high thermal flux in the Brasiliano-Pan-African orogeny: Implications for the geodynamic evolution of the Mantiqueira Province. *Precambrian Research*, **260**:1-22. <http://dx.doi.org/10.1016/j.precamres.2014.12.018>
- Bhatt S., Rana V., Mamtani M.A. 2017. Deciphering relative timing of fabric development in granitoids with similar absolute ages based on AMS study (Dharwar Craton, South India). *Journal of Structural Geology*, **94**:32-46. <https://doi.org/10.1016/j.jsg.2016.11.002>
- Borradaile G.J., Gauthier D. 2003. Interpreting anomalous magnetic fabrics in ophiolite dikes. *Journal of Structural Geology*, **25**(2):171-182. [https://doi.org/10.1016/S0191-8141\(02\)00025-1](https://doi.org/10.1016/S0191-8141(02)00025-1)
- Borradaile G.J., Henry B. 1997. Tectonic applications of magnetic susceptibility and its anisotropy. *Earth-Science Review*, **42**(1-2):49-93. [https://doi.org/10.1016/S0012-8252\(96\)00044-X](https://doi.org/10.1016/S0012-8252(96)00044-X)
- Bouchez J.L. 1997. Granite is never isotropic: an introduction to AMS studies in granitic rocks. In: Bouchez J.L., Hutton D., Stephens W.E. (Eds.), *Granite: from segregation to emplacement fabrics*. Dordrecht: Kluwer Academic Publishing, p. 95-112.
- Bruto Neves B.B., Campos Neto M.C., Fuck R.A. 1999. From Rodinia to western Gondwana; an approach to the Brasiliano-Pan African cycle and orogenic collage. *Episodes*, **22**(3):155-166. <https://doi.org/10.18814/epiuius/1999/v22i3/002>
- Campos Neto M.C. 2000. Orogenic systems from southwestern Gondwana. In: Cordani U.G., Milani E.J., Thomaz Filho A., Campos D.A. (Eds.), *Tectonic Evolution of South America*. Rio de Janeiro: 31st International Geological Congress, p. 335-365.
- Cañón-Tapia E. 2001. Factors affecting the relative importance of shape and distribution anisotropy in rocks: theory and experiments. *Tectonophysics*, **340**(1-2):117-131. [https://doi.org/10.1016/S0040-1951\(01\)00150-0](https://doi.org/10.1016/S0040-1951(01)00150-0)
- Clemens J.D., Petford N., Mawer C.K. 1997. Ascent mechanism of granitic magmas: causes and consequences. In: Holness M.B. (Ed). *Deformation-enhanced Fluid Transport in the Earth's Crust and Mantle*. London, Chapman and Hall, p. 144-171.
- Corrêa Neto A.V., Dayan H., Valença J.G. 1994. Intrusões sin-tectônicas em ambientes transpressivos: o exemplo do Plutonito Sapucaia na zona de cisalhamento do rio Paraíba do Sul. In: Congresso Brasileiro de Geologia, 38., 1994. *Boletim de Resumos Expandidos...* Balneário de Camboriú: SBG/DNPM/CPRM. v. 1. p. 160-161.
- Corrêa Neto A.V., Dayan H., Valença J.G., Cabral A.R. 1993. Geologia e estrutura da zona de cisalhamento do rio Paraíba do Sul e adjacências, no trecho entre Três Rios (RJ) e Sapucaia (RJ). In: Simpósio de Geologia do Sudeste, Rio de Janeiro. *Atas...* Rio de Janeiro: SBG, p. 194-200.
- Debon F., Le Fort P. 1983. A Chemical-Mineralogical Classification of Common Plutonic Rocks and Associations. *Transactions of the Royal Society of Edinburgh: Earth Sciences*, **73**(3):135-149. <http://dx.doi.org/10.1017/S0263593300010117>
- Dunlop D.J. 2002. Theory and application of the Day plot (Mrs/Ms vs Hcr/Hc). 1. Theoretical curves and tests using titanomagnetite data. *Journal of Geophysical Research*, **107**(B3):EPM 5-1-EPM 5-15. <https://doi.org/10.1029/2001JB000487>
- Egydio-Silva M., Mainprice D. 1999. Determination of stress directions from plagioclase fabrics in high grade deformed rocks (Além Paraíba shear zone, Ribeira fold belt, southeast Brazil). *Journal of Structural Geology*, **21**(12):1751-1771. [https://doi.org/10.1016/S0191-8141\(99\)00121-2](https://doi.org/10.1016/S0191-8141(99)00121-2)
- Esmaily D., Bouchez J.L., Siqueira R. 2007. Magnetic fabrics and microstructures of the Jurassic Shah-Kuh granite pluton (Lut Block, Eastern Iran) and geodynamic inference. *Tectonophysics*, **439**(1-4):149-170. <https://doi.org/10.1016/j.tecto.2007.04.002>
- Gaillot P., Saint-Blanquat M., Bouchez J.-L. 2006. Effects of magnetic interactions in anisotropy of magnetic susceptibility: Models, experiments and implications for igneous rock fabrics quantification. *Tectonophysics*, **418**(1-2):3-19. <https://doi.org/10.1016/j.tecto.2005.12.010>
- Heilbron M., Eirado L.G., Almeida J. 2016. *Mapa geológico e de recursos minerais do estado do Rio de Janeiro*. Escala 1:400.000. Belo Horizonte: CPRM.
- Heilbron M., Machado N. 2003. Timing of terrane accretion in the neoproterozoic-Eopaleozoic Ribeira Orogen (SE Brazil). *Precambrian Research*, **125**(1-2):87-112. [http://dx.doi.org/10.1016/S0301-9268\(03\)00082-2](http://dx.doi.org/10.1016/S0301-9268(03)00082-2)
- Heilbron M., Pedrosa Soares A.C., Campos Neto M.C., Silva L.D., Trouw R.A.J., Janasi V.D.A. 2004. Província Mantiqueira. In: Mantesso-Neto V., Bartorelli A., Carneiro C.D.R., Brito-Neves B.B. (Eds.), *Geologia do Continente Sul-Americano: evolução da obra de Fernando Flávio Marques de Almeida*. Rio de Janeiro: Beca, p. 203-235.
- Heilbron M., Tupinambá M.A., Valeriano C.M., Armstrong R., Eirado Siva L.G., Melo R.S., Simonetti A., Pedrosa Soares A.C., Machado N. 2013. The Serra da Bolívia complex: the record of a new Neoproterozoic arc-related unit at Ribeira belt. *Precambrian Research*, **238**:158-175. <http://dx.doi.org/10.1016/j.precamres.2013.09.014>
- Herro-Bervera J.-H. (Ed.). 2006. *Anisotropy of Magnetic Susceptibility Studies: From Microscopic to Continental Scales*. Tectonophysics Special Issue. Amsterdam: Elsevier, 418, issues 1-2, 162 p.
- Jackson M. 1991. Anisotropy of magnetic remanence: A brief review of mineralogical sources, physical origins, and geological applications, and comparison with susceptibility anisotropy. *Pure and Applied Geophysics*, **136**(1):1-28. <https://doi.org/10.1007/BF00878885>

- Jackson M., Sprowl D., Ellwood B. 1989. Anisotropies of partial anhysteretic remanence and susceptibility in compacted black shales: Grain-size- and composition-dependent magnetic fabric. *Geophysical Research Letters*, **16**(9):1063-1066. <https://doi.org/10.1029/GL016i009p01063>
- Jelinek V. 1981. Characterization of the magnetic fabric of rocks. *Tectonophysics*, **79**(3-4):T63-T67. [https://doi.org/10.1016/0040-1951\(81\)90110-4](https://doi.org/10.1016/0040-1951(81)90110-4)
- Machado N., Valladares C.S., Heilbron M., Valeriano C.M. 1996. U-Pb geochronology of the central Ribeira belt (Brazil) and implications for the evolution of the Brazilian orogeny. *Precambrian Research*, **79**(3-4):347-361. [http://dx.doi.org/10.1016/0301-9268\(95\)00103-4](http://dx.doi.org/10.1016/0301-9268(95)00103-4)
- Machado R., Demange M. 1994. Classificação Estrutural e Tectônica dos Granitóides Neoproterozóicos do Cinturão Paraíba do Sul no Estado do Rio de Janeiro. *Boletim IG-USP. Série Científica*, **25**:81-96. <http://dx.doi.org/10.11606/issn.2316-8986.v25i0p81-96>
- Machado R., Demange M., McReath I., Moutte J. 2000. Crustal zoning of Neoproterozoic pre-collisional granitoids in the Paraíba do Sul belt, Rio de Janeiro, Brazil. In: Brazilian Contribution to 31 International Geological Congress, Rio de Janeiro, Brazil. *Revista Brasileira de Geociências*. p. 70-73.
- Machado R., Endo I. 1993. A megaestrutura em flor positiva do vale do rio Paraíba do Sul no Rio de Janeiro. In: Simpósio de Geologia do Sudeste, 3., 1993, Rio de Janeiro. *Atas...* Rio de Janeiro, p. 208-213.
- Machado R., Philipp R.P., McReath I., Peucat J.J. 2016. Geochemical and isotopic evidence for the petrogenesis and emplacement tectonics of the Serra dos Órgãos batholith in the Ribeira belt, Rio de Janeiro, Brazil. *Journal of South American Earth Sciences*, **68**:187-204. <https://doi.org/10.1016/j.jsames.2016.01.005>
- Mamtani M.A. 2014. Magnetic fabric as a vorticity gauge in syntectonically deformed granitic rocks. *Tectonophysics*, **629**:189-196. <https://doi.org/10.1016/j.tecto.2014.01.032>
- Martín-Hernández F., Cañon-Tapia E., Mattei M., Bijaksana S. (Eds.). 2009. *Magnetic Anisotropy from Different Scales to Different Parameters*. Tectonophysics Special Issue. Amsterdam: Elsevier, 466, issues 1-2, 134 p.
- Martín-Hernández F., Lüneburg C.M., Aubourg C., Jackson M. (Eds.). 2004. Magnetic fabric: methods and applications — an introduction. *Geological Society, London, Special Publications*, **238**(1):1-7. <https://doi.org/10.1144/GSL.SP.2004.238.01.01>
- Nummer A.R. 2001. *Geometria e cinemática de alojamento do maciço granítico Arrozal, sudoeste do Estado do Rio de Janeiro, RJ*. Thesis, Universidade de São Paulo, São Paulo, 210 p.
- Nummer, A.R., Machado, R., Dehler, N.M. 2007. Pluton emplacement in a releasing bend in a transpressive regime: the Arrozal granite in the Paraíba do Sul shear belt, Rio de Janeiro. *An. Acad. Bras. Ciência*. Rio Janeiro. v. 79 (2), p.299-305.
- Oliva-Urcia B., Larrasoña J.C., Pueyo E.L., Gil A., Mata P., Parés J.M., Schleicher A.M., Pueyo O. 2009. Disentangling magnetic subfabrics and their link to deformation processes in cleaved sedimentary rocks from the Internal Sierras (west central Pyrenees, Spain). *Journal of Structural Geology*, **31**(2):163-176. <https://doi.org/10.1016/j.jsg.2008.11.002>
- Paterson S.R., Fowler Jr. T.K., Schmidt K.L., Yoshinobu A.S., Yuan E.S., Miller R.B. 1998. Interpreting magmatic fabric patterns in plutons. *Lithos*, **44**(1-2):53-82. [https://doi.org/10.1016/S0024-4937\(98\)00022-X](https://doi.org/10.1016/S0024-4937(98)00022-X)
- Pinto C.P. (Coord.). 1980. *Projeto Carta geológica do Estado do Rio de Janeiro (DRM) - Folhas Anta, Duas Barras, Teresópolis e Nova Friburgo*. Relatório Final. Belo Horizonte: Geosol Geologia e Sondagens Ltda. v. 1. p. 237-265.
- Raeisi D., Mirnejad H., Sheibi M. 2019. Emplacement mechanism of the Tafresh granitoids, central part of the Urumieh–Dokhtar Magmatic Arc, Iran: evidence from magnetic fabrics. *Geological Magazine*, **156**(9):1510-1526. <https://doi.org/10.1017/S0016756818000766>
- Raposo M.I.B., Drukas C.O., Basei M.A.S. 2014. Deformation in rocks from Itajaí basin, Southern Brazil, revealed by magnetic fabrics. *Tectonophysics*, **629**:290-302. <https://doi.org/10.1016/j.tecto.2013.12.019>
- Raposo M.I.B., Gastal M.C.P. 2009. Emplacement mechanism of the main granite pluton of the Lavras do Sul intrusive complex, South Brazil, determined by magnetic anisotropies. *Tectonophysics*, **466**(1-2):18-31. <https://doi.org/10.1016/j.tecto.2008.10.015>
- Raposo M.I.B., McReath I., D'Agrella-Filho M.S. 2006. Magnetic fabrics, rock magnetism, Cathodo-luminescence and petrography of “undeformed” Bambuí Limestones from São Francisco basin (Minas Gerais State-Brazil): an integrated study. *Tectonophysics*, **418**(1-2):111-130. <https://doi.org/10.1016/j.tecto.2005.12.016>
- Raposo M.I.B., Pressi L.F., Assis Janasi V. 2012. Magnetic fabrics and their relationship with the emplacement of the Piracéia pluton, SE Brazil. *International Journal of Earth Sciences*, **101**(3):773-786. <https://doi.org/10.1007/s00531-011-0696-5>
- Román-Berdiel T., Pueyo-Morer E.L., Casas-Sainz A.M. 1995. Granite emplacement during contemporary shortening and normal faulting: structural and magnetic study of the Veiga Massif (NW Spain). *Journal of Structural Geology*, **17**(12):1689-1706. [https://doi.org/10.1016/0191-8141\(95\)00062-1](https://doi.org/10.1016/0191-8141(95)00062-1)
- Sheibi M., Majidi P. 2015. Emplacement mechanism of the Challu granitoids pluton using magnetite fabric method, southern Damghan. *Geosciences*, **24**(95):87-98.
- Silva L.C. (Coord.). 2000. *Geologia do Estado do Rio de Janeiro: texto explicativo do mapa geológico do Estado do Rio de Janeiro*. Escala 1:400.000. Brasília: CPRM.
- Silva L.C., McNaughton J.N., Armstrong R., Hartmann L.A., Fletcher I.R. 2005. The neoproterozoic Mantiqueira Province and its African connections: a zircon-based U-Pb geochronologic subdivision for the Brasiliano/Pan-African systems of orogens. *Precambrian Research*, **136**(3-4):203-240. <http://dx.doi.org/10.1016/j.precamres.2004.10.004>
- Silva L.C., McNaughton J.N., Hartmann L.A., Fletcher I.N.R. 2003. Zircon U-Pb SHRIMP dating of the Serra dos Órgãos and Rio de Janeiro Gneissic granitic suites: Implications for the (560 ma) Brasiliano/Pan-African collage. *Revista Brasileira de Geociências*, **33**(2):237-244.
- Stephenson A., Sadikun S., Potter D.K. 1986. A theoretical and experimental comparison of the anisotropies of magnetic susceptibility and remanence in rocks and minerals. *Geophysical Journal International*, **84**(1):185-200. <https://doi.org/10.1111/j.1365-246X.1986.tb04351.x>
- Stipp M., Stünitz H., Heilbronner R., Schmid S.M. 2002. The eastern Tonale fault zone: a “natural laboratory” for crystal plastic deformation of quartz over a temperature range from 250 to 700°C. *Journal of Structural Geology*, **24**(12):1861-1884. [https://doi.org/10.1016/S0191-8141\(02\)00035-4](https://doi.org/10.1016/S0191-8141(02)00035-4)
- Tarling D.H., Hrouda F. 1993. *The magnetic anisotropy of rocks*. London; New York: Chapman & Hall.
- Trindade R.I.F., Raposo M.I.B., Ernesto M., Siqueira R. 1999. Magnetic susceptibility and partial anhysteretic remanence anisotropies in the magnetite-bearing granite pluton of Tourão, NE Brazil. *Tectonophysics*, **314**(4):443-468. [https://doi.org/10.1016/S0040-1951\(99\)00220-6](https://doi.org/10.1016/S0040-1951(99)00220-6)
- Trouw R.A.J., Heilbron M., Ribeiro A., Paciullo F., Valeriano C.M., Almeida J.C.H., Tupinamba M.A., Andreis R.R. 2000. The central segment of the Ribeira belt. In: Cordani U.G., Milani E.J., Thomaz Filho A., Campos D.A. (Eds.), *Tectonic Evolution of South America*. Rio de Janeiro, 31st International Geological Congress, p. 287-310.
- Trubač J., Žák J., Chlupáčová M., Janoušek V. 2009. Magnetic fabric of the Řičany granite, Bohemian Massif: A record of helical magma flow? *Journal of Volcanology and Geothermal Research*, **181**(1):25-34. <https://doi.org/10.1016/j.jvolgeores.2008.12.005>
- Tupinambá M. (Coord.). 2012a. *Geologia e recursos minerais da folha Nova Friburgo (CPRM) SF.23-Z-B-II, estado do Rio de Janeiro*. Escala 1:100.000. Belo Horizonte: CPRM, 136 p.
- Tupinambá M. 2012b. *Nota explicativa do Mapa Geológico da Folha Nova Friburgo 1:100.000*. Rio de Janeiro: CPRM — Serviço Geológico do Brasil, 136 p.
- Tupinambá M. 1999. *Evolução tectônica e magmática da Faixa Ribeira na região da Serra dos Órgãos*. Thesis, Instituto de Geociências, Universidade de São Paulo, São Paulo, 186 p.
- Tupinambá M.A., Heilbron M., Valeriano C.M., Porto Júnior R., de Dios F.B., Machado N., Silva L.G. do E., de Almeida J.C.H. 2012. Juvenile contribution of the Neoproterozoic Rio Negro magmatic arc (Ribeira Belt, Brazil): Implications for western Gondwana amalgamation. *Gondwana Research*, **21**(2-3):422-438. <http://dx.doi.org/10.1016/j.gr.2011.05.012>
- Villaseca C., Barbero L., Herreros V. 1998. A re-examination of the typology of peraluminous granite types in intracontinental orogenic belts. *Transactions of the Royal Society of Edinburgh: Earth Sciences*, **89**(2):113-119. <http://dx.doi.org/10.1017/S0263593300007045>